SCIENTIFIC REPORTS

OPEN

SUBJECT AREAS:
TWO-DIMENSIONAL MATERIALS
NANOPARTICLES
SELF-ASSEMBLY
SOLAR CELLS

Received
7 June 2013

Accepted
4 October 2013

Published
21 October 2013

Correspondence and requests for materials should be addressed to C.K.H. (hongck@chonnam.ac.kr)

Surfactant free most probable TiO_2 nanostructures via hydrothermal and its dye sensitized solar cell properties

Sawanta S. Mali[1], Hyungjin Kim[1], Chang Su Shim[1], Pramod S. Patil[2,3], Jin Hyeok Kim[2] & Chang Kook Hong[1]

[1]School of Applied Chemical Engineering, Chonnam National University, Gwangju, 500-757 (South Korea), [2]Deparment of Materials Science and Engineering, Chonnam National University, Gwangju, 500-757, (South Korea), [3]Thin Film Materials Laboratory, Department of Physics, Shivaji University, Kolhapur, India 416 004.

Tailoring the nano-morphology and nano-architecture of titanium dioxide (TiO_2) is the most important task in the third generation solar cells (Dye sensitized solar cells/Quantum dot sensitized solar cells) (DSSCs/QDSSCs). In this article we present complete study of surfactant free synthesis of TiO_2 nanostructures by a simple and promising hydrothermal route. The plethora of nanostructures like nanoparticles clusters, 1D tetragonal nanorods, 3D dendrites containing nanorods having <30 nm diameter and 3D hollow urchin like have been synthesized. These nanostructures possess effective large surface area and thus useful in DSSCs. In the present work, 7.16% power conversion efficiency has been demonstrated for 3D dendritic hollow urchin like morphology. Our synthetic strategy provides an effective solution for surfactant free synthesis of efficient TiO_2 nanoarchitectures.

After the discovery of photoelectrochemical properties of nanostructured titanium oxide (TiO_2), it is recognized as one of most promising wide band gap semiconducting materials for photocatalysis, dye/quantum dot sensitized solar cells (DSSCs/QDSSCs) and lithium ion batteries[1–6]. The DSSC is a molecular approach to photovoltaic solar energy conversion technology. This is one of the emerging photovoltaic technologies that offer the potential to reduce the cost of photovoltaic electricity production. During the past two decades, nanoporous polycrystalline titania has been extensively used in DSSCs, which demonstrated to be a promising alternative to silicon based solar cells due to their relatively high solar-to-electric power conversion efficiency at low cost. The transportation of electrons through TiO_2 film and effective dye loading are the most important parameters in DSSCs. These two parameters depend upon the surface topography of the photoanode, surface area, grain boundaries between two nanostructures and porosity of the photoanodes. Hence, the tailoring nanomorphology of photoanode is a key factor in the DSSCs application[2].

TiO_2 mainly occurs in three main crystal phases: anatase, rutile and brookite. However, synthesis of one/three dimensional (1D/3D) growth of any one of these nanostructures is a difficult task. Recently many attempts have been made to tackle this problem using strong acid reaction[7], ionic liquid surfactant mediator[8], dissolve and grow process[9]. Recently, D.-B. Kuang *et al.* have developed a new oriented hierarchical single crystalline anatase TiO_2 nanowire arrays, tri-functional spheres consisting nanorods and hierarchical nanowire trunks by hydrothermal process[10–12]. C. Lin *et al.* reported porous rutile TiO_2 nanorod arrays etching process[13]. However till now there is no substantial work on surfactant free hydrothermal process for synthesis of nanostructured TiO_2 using Titanium butoxide ($Ti(OC_4H_9)_4$) (TBT) precursor. On the other hand 1D nanostructures provide slow recombination rate, fast electron transport and effective light scattering ability within the nanostructures. The 3D nanostructure like nanoflowers[14], hierarchical microspheres[15,16] functioning high specific surface area results in an effective dye adsorptive and light-scattering layer. To achieve this we have developed surfactant free hydrothermal synthesis route for 1D as well as 3D TiO_2 nanostructures with well-defined shape and size. Such novel 1D nanorods arrays with 3D dendrites and hollow urchin provide not only effective surface area but are also helpful for effective light harvesting in DSSCs. The present study is focused on the effect of temperature on hydrolysis of TBT precursor for tuning of TiO_2 nanomorphology and its DSSCs performance discussed systematically. The key innovation in the present study is to demonstrate surfactant free tuning of the nanomorphology of TiO_2 nanostructures by a controlled single step hydrothermal process at various system temperatures. The TBT was controlled hydrolyzed

in hydrochloric acid and distilled water (1 : 1 v:v). The reaction temperature was varied from 100°C to 190°C and growth mechanism is studied systematically. Finally these nanostructures were used for DSSCs application.

Results

Figure 1 shows typical FESEM images of TiO_2 nanostructures synthesized at different reaction temperatures. The reaction time was 3 h for each sample deposition. Figure 1 (a) show the FESEM images

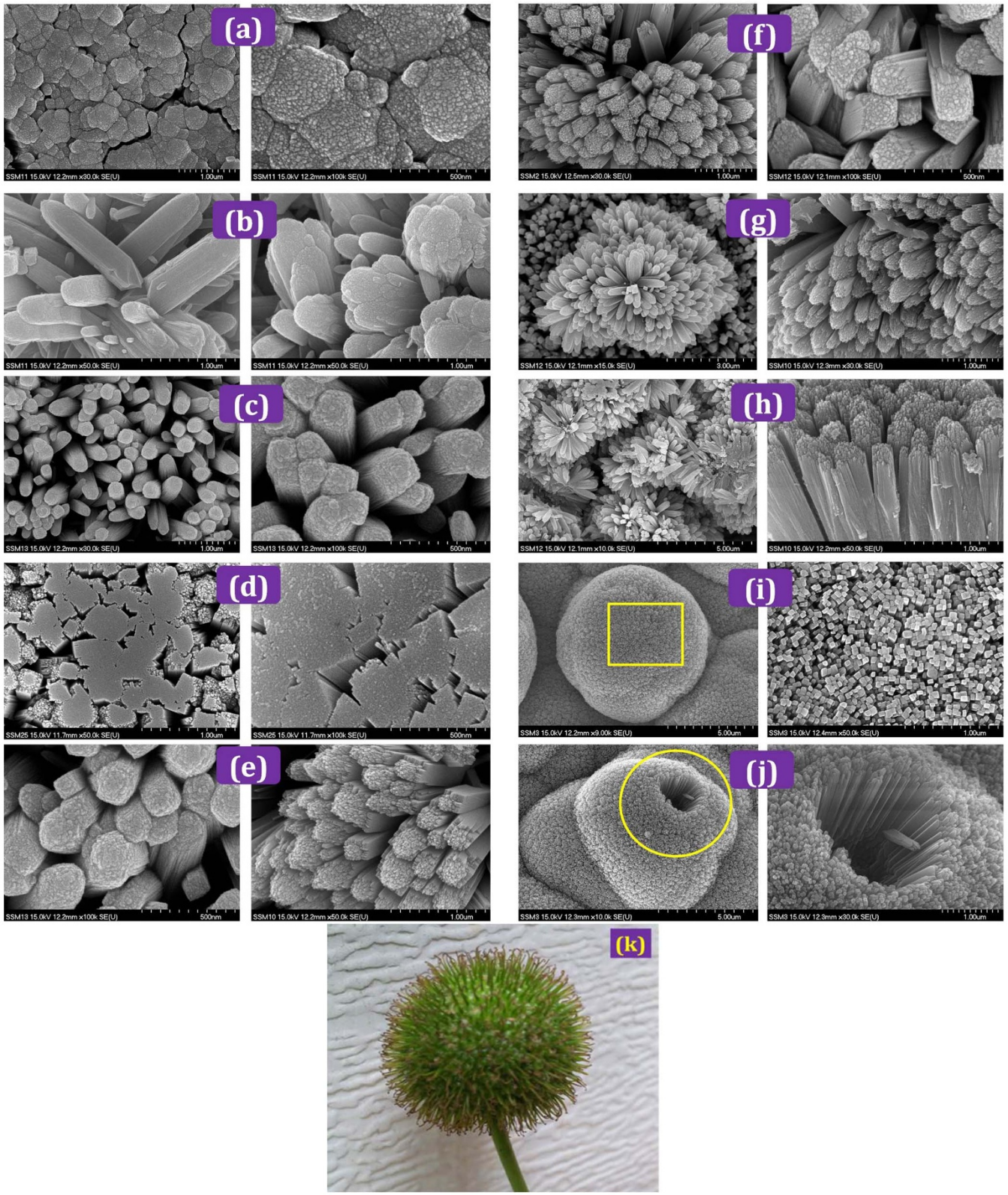

Figure 1 | Exotic Nanostructures of hydrothermally grown 1D/3D TiO_2 at different hydrolysis conditions. (a) T_{100}, (b) T_{110}, (c) T_{120}, (d) T_{130}, (e) T_{140}, (f) T_{150}, (g) T_{160}, (h) T_{170}, (i) T_{180} and (j) T_{190}. The images on right hand show their respective highly magnified FESEM micrographs. (k) Photograph of a hollow platanus seed found in the nature that mimics the nanostructures of T_{190} sample. (Image Credit: Dr. Sawanta S. Mali).

of TiO_2 synthesized at 100°C (T_{100}) on the FTO coated conducting substrate. The compact TiO_2 nanoparticles clusters are deposited on entire surface of the FTO substrate. The particle sizes of the deposited nanoparticles were found to be 25–35 nm. Figure 1 (b) show FESEM images of TiO_2 sample at 110°C (T_{110}), revealing tapered nanorods having 180 nm diameter. However, the highly magnified image shows that these large size nanorods are made up from agglomeration of number of small nanorods (pillars). Therefore we have decided to increase the hydrothermal system temperature. Figure 1 (c) show FESEM images of TiO_2 nanorods deposited at 120°C designated as T_{120}. Uniform distribution of vertically aligned nanorods covered throughout the substrate. Figure 1 (d) show the sample morphology deposited at 130°C (T_{130}). The previously agglomerated nanorods start separating into much smaller (25–35 nm) nanorods. Figure 1 (e) shows FESEM image of T_{140} sample. There are no drastic changes observed for T_{140} sample except small inter-nanostructure spacing. However T_{150} sample shows excellent inter-nanostructure separation between two bunches of nanorods (Figure 1 (f)). These nanorods are covered uniformly over entire surface having tetragonal shape with square top facets. Notably these tetragonal nanorods are vertically aligned to the FTO substrate (Please check electronic Supporting Information Figure S1 and Figure S2). The cross sectional FESEM image shows TiO_2 nanorods were uniformly distributed and aligned vertically to the FTO substrate. The thickness of deposited sample is ~6.6 μm throughout surface. The inset shows highly magnified FESEM image of selected area that reveals bunch of aligned nanorods. The TiO_2 nanorod and FTO interface is very smooth, which is beneficial for effective flow of electrons.

It is well known that the nanorods are tetragonal in shape with square top facets, the expected growth habit for the tetragonal crystal structure. Similar morphology has been observed by E. Hosono *et al.* and Z. L. Wang et al.[17,9] by hydrolysis of the $TiCl_3$ in NaCl solvent at 200°C and Ti foil surface etching process in strong acidic concentrated HCl solution on carbon nanofiber for ~18 h respectively. Moreover, S. A. Berhe *et al.*[18] also reported similar morphology by hydrolysis of titanium alkoxide in HCl solution by two consecutive 6 h growths on seed coated MoO_2 substrate. Here we could obtain same bundles of enclosing a few or several nanorods in relatively less time, using surfactant free solution and seed free substrate. The sample deposited at 160°C (i.e. Sample-T_{160}) shows novel nanoflower like morphology having bunch of aligned nanorods. The diameter of such flower is about 3 μm as shown Figure 1 (g). However, T_{170} sample shows well distributed TiO_2 nanoflowers over the substrate as shown in Figure 1 (h). The image on right hand side shows clearly these nanorods containing bunch of aligned nanorods. The cross section FESEM images shows the dendrites are tapered and centered at the core of the nanoflower (Please check supporting information Figure S3). These nanorods are single crystalline in nature confirmed by spotted SAED pattern[19–21].

E. Hosono *et al.*[17] and recently Z. L. Wang *et al.*[9] discussed the recrystallization process i.e. dissolve and grow process of TiO_2 nanostructures by hydrothermal process. The hydrolysis reaction in strong acidic media can be explained as follows:

$$2Ti + 6HCl \rightarrow 2TiCl_3 + 3H_2(g) \quad (1)$$

$$Ti^{3+} + H_2O \rightarrow TiOH^{2+} + H^+ \quad (2)$$

$$TiOH^{2+} + O_2^- \rightarrow Ti(IV) - oxo\ species + O_2^- \rightarrow TiO_2 \quad (3)$$

The XRD pattern of the TiO_2 sample deposited onto FTO substrate is shown in Figure S4 (Supporting Information Figure S4). The reflection peaks can be readily indexed to pure rutile TiO_2. The other peaks are originated from FTO substrate. The proposed formation of 1D nanorods growth is as follows:

Initially Ti species from TBT precursor start to react with H^+ ions from concentrated solution. It is well known that Ti^{3+} species are not stable in an aqueous solution, therefore $TiOH^{2+}$ species are formed by hydrolysis of Ti^{3+} species. According to the "dissolve and grow method[9,15,17] $TiOH^{2+}$ is oxidized to Ti(IV) by reaction with dissolved oxygen. The Ti(IV) complex ions are thus used as the growth units. The formation mechanism of the rutile TiO_2 NRs may be described as follows: For rutile TiO_2, a TiO_6 octahedron forms first by bonding of a Ti atom and six oxygen atoms. The TiO_6 octahedron then shares a pair of opposite edges with the next octahedron, forming a chain-like structure. Because the growth rate of the different crystal faces depends on the numbers of corners and edges of the coordination polyhedra available, the growth of rutile NRs follows the sequence $(110) < (100) < (101) < (001)$[17,22–24]. Thus, rutile TiO_2 NRs along [001] direction are formed. The nanorods are single crystalline, as evidenced by the sharp spotted SAED pattern of a nanorod examined along the [110] zone axis. The chemical stoichiometry of the nanorods was further examined with X-ray photoelectron spectroscopy (XPS) and the atomic ratio of Ti to O was found to be ~1:2 (Please check electronic Supporting Information, Figure S5).

Figure 1 (i) show the FESEM images of T_{180} sample. The deposited samples exhibit 3D dendritic TiO_2 nanostructures containing nanorods. These dendritic microspheres are ~7.5 μm in diameter. Interestingly the highly magnified image shows uniform distribution of tetragonal nanorods of ~25–35 nm diameter. Similar morphology has been reported by J. H. Kim *et al.*[25,26] with a composition of $100H_2O$:7HCl:0.03CTAB:0.05 0.01TTIP (where CTAB: Cetyl trimethylammonium bromide, TTIP: Titanium tetraixopropoxide) as a solution composition for 20 h hydrothermal process. In our case, after increasing the hydrothermal system temperature it is observed that the 3D dendritic nanostructured microspheres open at the outer surface (Figure 1 (j)). Such novel hollow urchin nanostructures have 1 μm diameter. This 3D dendritic hollow urchin structure may have formed due to selected surface etching of Ti species in strong acid medium at relatively higher temperature[7]. A magnified FESEM image of the sample in Figure 1 (j) shows that these 3D dendrites mimics the hollow platanus seed (Figure 1 (k)), with diameters of 1 μm and numerous nanorods (~30 nm) compactly growing around their surfaces.

The crystallinity of deposited samples was confirmed by SAED, TEM and HRTEM characterizations. Figure 2 show the TEM, SAED patterns and HRTEM images of selected TiO_2 samples: (a–e) Sample deposited at 140°C (T_{140}). (f–j) sample deposited at 160°C (T_{160}) and (k–o) sample deposited at 190°C (T_{190}). The T_{140} sample exhibits the nanorods with tapered morphology (Fig. 2(a)). The agglomerated tetragonal nanorods are separated at the upper side (head) while lower side (tail) is compact in nature. The highly magnified image of the tail (Figure 2 (b)) reveals bundles of tiny nanorods. The diameter of the tail side is ~80 nm.

Figure 2 (c) shows highly magnified TEM image of upper side (head) of the tetragonal nanorods. It is clear that the nanorods are separated at the head side with ~30 nm diameter of each nanorod. Moreover, these nanorods are single crystalline as confirmed by their SAED pattern (Figure 2 (d)). The clear lattice fringes of the single nanorod of the T_{140} sample is observed to be single crystalline along their entire length. The interplanar spacing obtained from the HRTEM lattice fringes along d_{110} = 0.32 nm between the adjacent lattice fringes perpendicular to the rod axis can be assigned to the rutile TiO_2 (110). The lattice spacing of d_{001} = 0.29 nm along the longitudinal axis direction pertains to the d-spacing of rutile TiO_2 (001) crystal planes[14]. Figure 2 (f–j) presents the TEM images of T_{160} sample. These images are almost similar to sample T_{140} however the separation of the upper side is slight higher. Also similar lattice spacings along [110] and [001] directions have been observed. Figure 2 (k–o) shows the TEM images of the T_{190} sample. The SAED pattern shows single crystalline nature of the 3D hollow urchin like

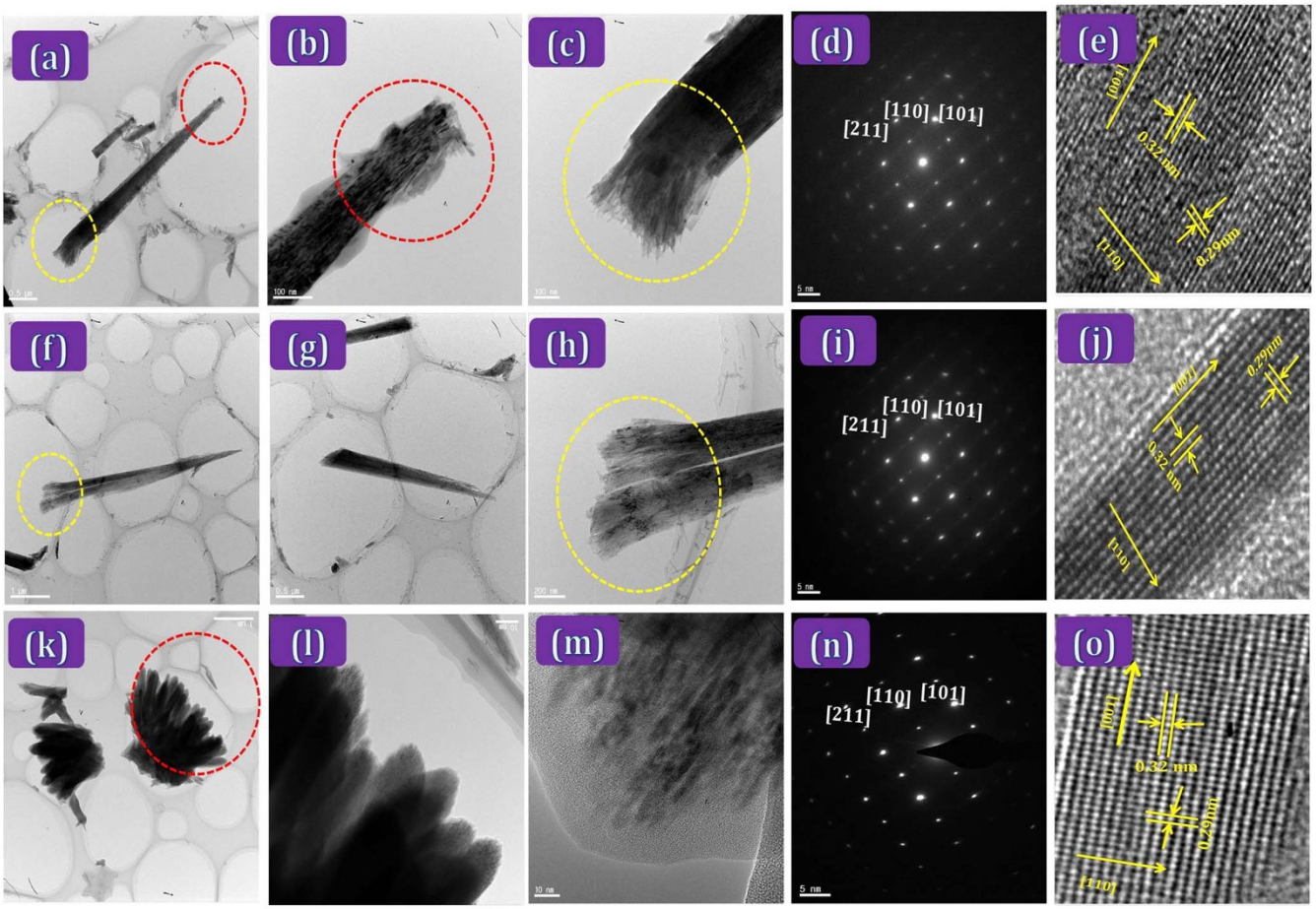

Figure 2 | Transmission Electron Microscopic (TEM) images, selective area diffraction (SAED) patterns and high resolution transmission electron microscopic images (HRTEM) of selected TiO_2 samples: (a–e) Sample deposited at 140°C (T_{140}). (f–j) sample deposited at 160°C (T_{160}) and (k–o) sample deposited at 190°C (T_{190}).

morphology of the sample (T_{190}). The growth direction of the tetragonal nanorods in the 3D TiO_2 dendrites were in [001] direction, which is the same as for the 1D vertically grown nanorods. The exposed surfaces of the nanorods were {110} facets[25]. Interestingly it is observed that the crystallinity of the T_{190} sample is better than other samples.

From the above discussion the possible growth mechanism of nanoparticles-to-nanorods-to-3D dendrite microspheres-to-3D hollow urchin-like architectures is represented in Figure 3. Here we have used strong acid approach for the synthesis of 1D and 3D nanostructures. It is well known that the equal volume of HCl:H_2O is beneficial for the synthesis of aligned TiO_2 nanorods[7,21]. In our procedure we have kept HCl:H_2O (1 : 1 v:v) fixed throughout the experiments. The concentrated HCl constraint on the hydrolysis of the TiO_2 precursor results in 1D TiO_2 nanorods. The growth of oriented TiO_2 nanorods requires slow hydrolysis of TBT in a fairly strong acidic aqueous medium. However the system temperature also plays a key role in the complete hydrolysis of titanium precursor. At 100°C (T_{100}) insufficient system temperature causes creation of clusters of nanoparticles. When the FTO substrates were immersed in the reaction solutions, titanium precursor would condense on the FTO surface and growth of TiO_2 seeds starts[26]. At 130°C (T_{100} sample), pillars of aligned nanorods are formed due to controlled hydrolysis. The increase rate of hydrolysis facilitates rapid formation of nanorods that causes 3D growth of bunch of nanorods, at 160°C (T_{160}) and 170°C (T_{170}). However, drastic modification has been observed for T_{180} sample. The 3D spherical dendrites of diameter ~7.5 μm containing nanorods of size ~30 nm have been formed. Similar microstructures have been synthesized by J. H. Kim *et al.*[25]. using 100H_2O:7HCl:0.03CTAB:0.05TTIP. Here authors have used CTAB as a surfactant and concluded that the surfactant is helpful for the aligned growth of TiO_2 nanorods. However it is also concluded that such common surfactants are not playing major role in the tuning and reproducibility of nanomorphology[7].

At 190°C, the sufficiently high temperature causes formation of 3D hollow urchin like morphology due to higher surface energy. The low magnified FESEM image shows uniformity of the hollow urchin structure. (Supporting information Figure S6).

Further the statistical distribution of nanorod diameter of 3D dendritic sample is estimated. Figure 4 shows a statistical histogram of the diameter distribution of the hydrothermally grown 3D TiO_2 dendrites. The inset shows the selected area for this measurement. It is clear that the large numbers of 1D nanorods are in the range of 25–30 nm.

The DSSC based on 3D nanostructures like nanoflowers[8], hierarchical microspheres[9,10] result in high surface area and susequently enable effective dye adsorptiion. Recently Z. Sun *et al.* demonstrated nanowire/dendritic 3D nanostructures useful for effectively light harvesting in DSSCs. These 1D-3D nanostructures show 7.2% photon conversion efficiency (PCE). Therefore, 3D nanostructures combined with 1D nanostructures has opened a new approach towards efficient DSSCs[27]. Therefore we have decided to use such 1D/3D nanostructure in well-known DSSC application. The DSSC devices in this study were fabricated by following standard procedure[10]. The N-719 dye was used for sensitization and Pt/FTO was used as a counter electrode. The samples show good solar cell properties

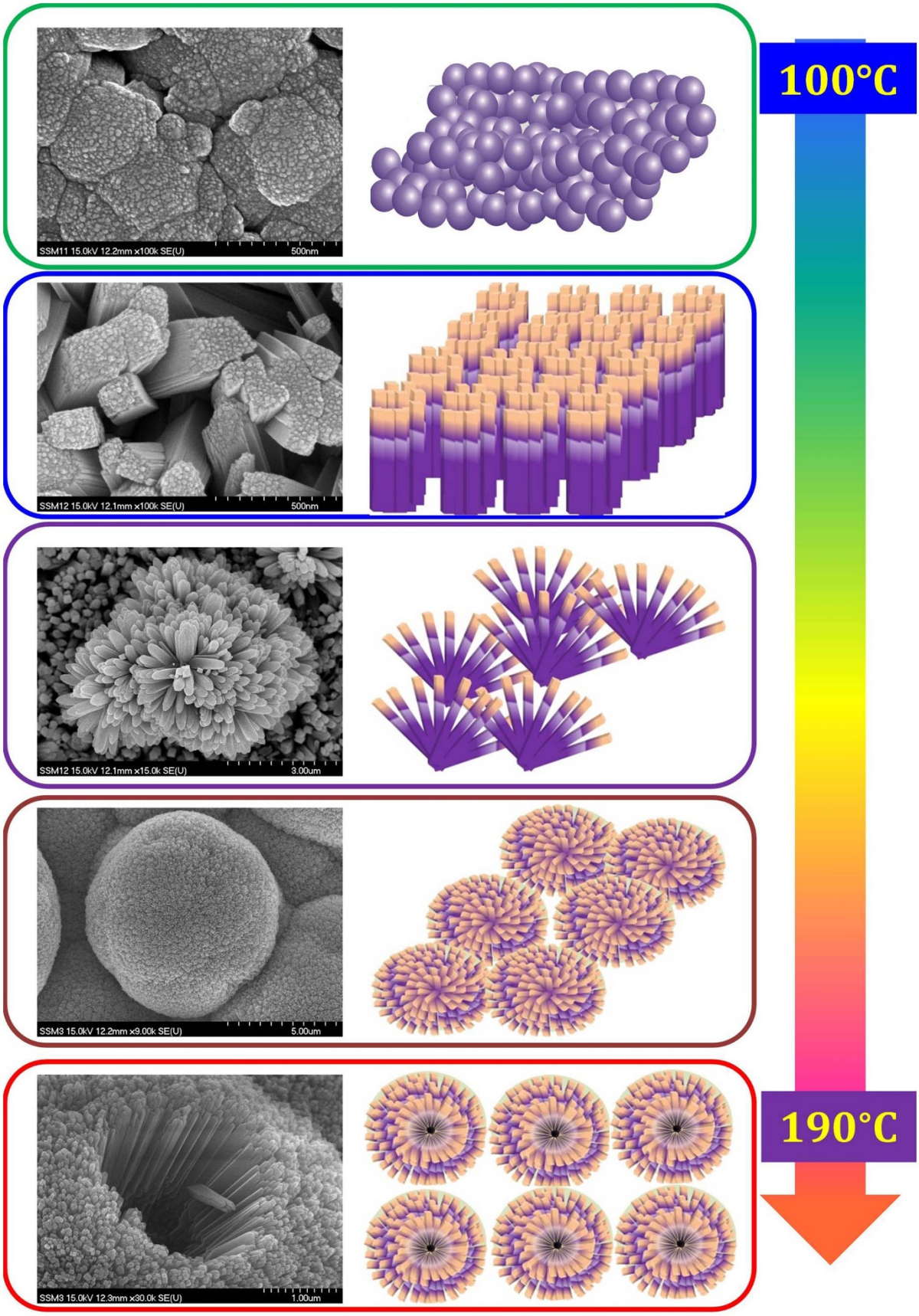

Figure 3 | **FESEM images of the nanostructured TiO_2 obtained at different temperature from 100°C to 190°C. The figures on right hand show their corresponding possible growth mechanism.**

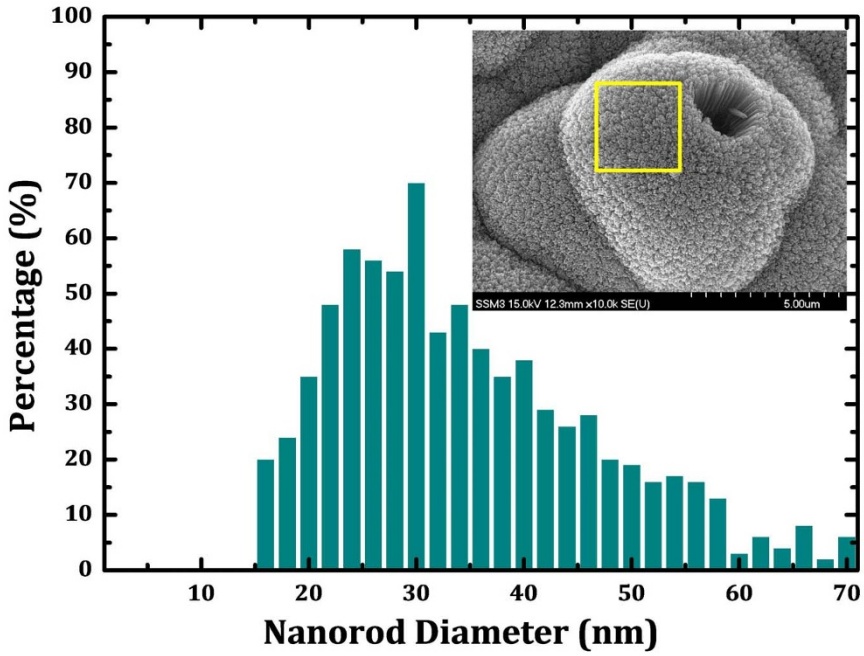

Figure 4 | Statistical histogram displays the diameter distribution of the TiO_2 nanorods in opal urchin dendrite. Inset shows the selected area for the nanorods diameter measurement.

under 100 mW/cm^2 AM 1.5 illumination and the results are summarized in Table 1.

Figure 5 shows the J-V curves of TiO_2 sample based on different morphologies. For nanoparticle T_{100} sample based DSSC cell short-circuit current density (J_{SC}), open-circuit voltage (V_{OC}), fill factor (FF), and efficiency (η) were J_{SC} = 7.85 mAcm^{-2}, Voc = 0.587 V, FF = 48.2, and η = 2.34%, respectively. DSSC device based of T_{110} sample shows J_{SC} = 9.42 mAcm^{-2}, V_{OC} = 0.589 V, FF = 54, and η = 2.99%. Sample T_{120} shows 3.86% conversion efficiency with 9.53 mAcm^{-2} Jsc and 0.599 V_{OC} respectively. Interestingly it was found that the current density (9.79 mAcm^{-2}) as well as efficiency (4.11%) of the T_{130} sample is larger than nanoparticulate clusters and compact nanorods pillars. This may be due to higher surface area beneficial for effective dye loading. The T_{140} sample shows slightly higher 4.14% conversion efficiency. The T_{150} sample shows V_{OC} = 0.610 V, J_{SC} = 12.59 mAcm^{-2}, FF = 61.1 and η = 4.93%. While the 3D TiO_2 nanoflower sample shows drastic enhancement in power conversion efficiency. These 3D nanoflowers (Sample-T_{160}) exhibit η = 5.16% with V_{OC} = 0.609 V, J_{SC} = 13.22 mAcm^{-2} and FF = 60.9. This enhancement is due to effective light scattering between the 3D flowers. Further T_{170} sample shows slightly higher efficiency (5.32%). However, the 3D dendritic urchin samples (T_{180} and T_{190} hollow urchin) exhibit drastic enhancement in current density from 12.83 mAcm^{-2} to 12.98 mAcm^{-2} and 17.17 mAcm^{-2} respectively. The power conversion efficiency of the T_{190} sample is 7.16% with V_{OC} = 0.612 V and FF = 64.7. This morphology offers higher surface area and unique morphology that facilitates scattering of light and effective light harvesting.

The incident-photon-to-current conversion efficiency (IPCE) spectra would offer detailed information on the effective light harvesting capability of the DSSCs based on TiO_2 samples. Figure 6 shows the IPCE spectra as a function of wavelength for T_{100} (●) and T_{190} (●) samples. The IPCE spectrum of N719-Dye loaded T_{190} device shows maximum absorption at approximately 535 nm, which is attributed to the contribution of effective dye loading. The 3D dendritic hollow urchin sample exhibits 83% IPCE at 535 nm while T_{100} sample shows only ~42% IPCE. The T_{190} sample shows a higher IPCE from 350 nm to 700 nm wavelength range than T_{100} sample, which correlate well with increased photocurrent density values.

Table 1 | Solar cell parameters obtained from TiO_2 samples deposited at different temperatures recorded under illumination of simulated solar light (100 mW cm^{-2}, AM 1.5 G)

Sample	Voc (V)	Jsc (mAcm^{-2})	FF (%)	η (%)
T_{100}	0.587	7.85	48.2	2.34
T_{110}	0.589	9.42	54.0	2.99
T_{120}	0.599	9.53	64.3	3.86
T_{130}	0.608	9.79	65.5	4.11
T_{140}	0.613	10.15	63.0	4.14
T_{150}	0.610	12.59	61.1	4.93
T_{160}	0.609	13.22	60.9	5.16
T_{170}	0.610	12.83	64.5	5.32
T_{180}	0.617	12.98	65.0	5.43
T_{190}	0.612	17.17	64.7	7.16

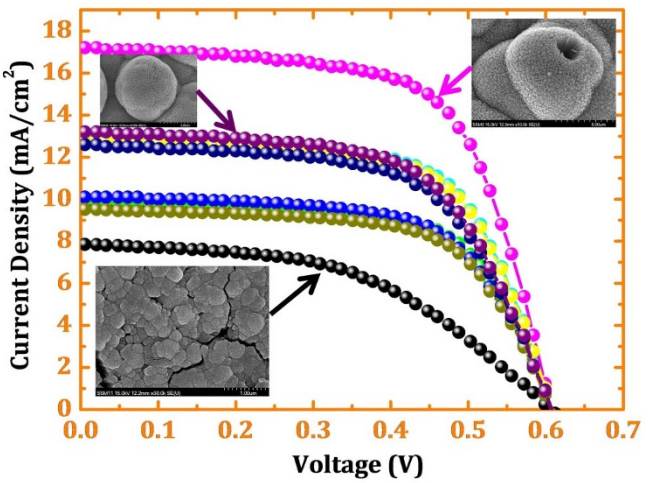

Figure 5 | J-V curves of hydrothermally grown TiO_2 samples at different temperatures.

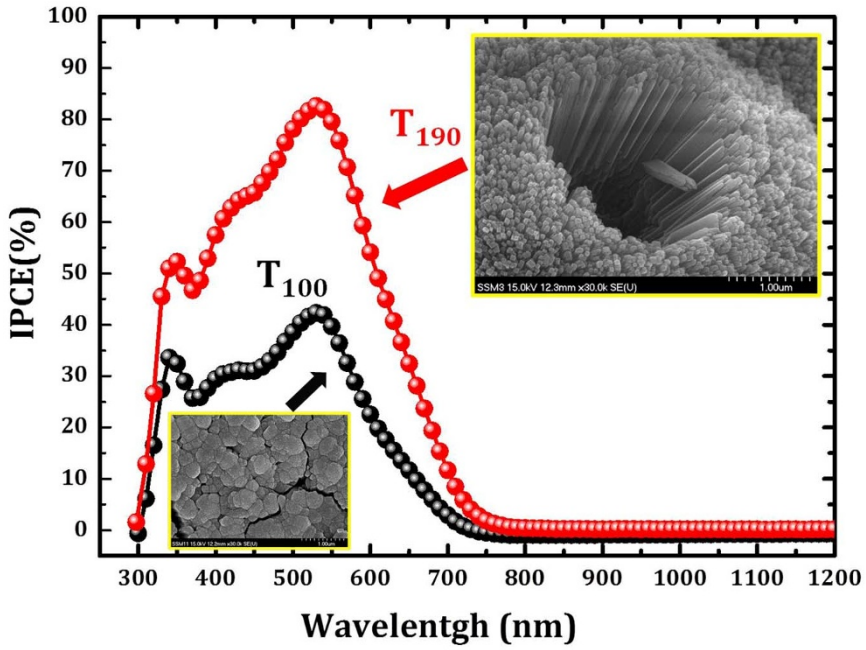

Figure 6 | Incident photon-to-current conversion efficiency (IPCE) spectra of T_{100} (●) nanoparticulate and T_{190} (●) 3D dendritic hollow urchin samples.

The Jsc values have been estimated by using following IPCE equation[28]

$$J_{SC}\Big/ mAcm^{-2} = \frac{hc}{q}\int_{\lambda_1}^{\lambda_2}\frac{P_{in\lambda}\times EQE_{\lambda}\times d\lambda}{\lambda} \qquad (4)$$

where h is Planck's constant (Js^{-1}), c is the speed of light in vacuum (ms^{-1}), and λ_1 and λ_2 (nm) are the limits of the active spectrum of the device. P incident photon flux density at wavelength λ. The external quantum efficiency (EQE) of the hydrothermally grown TiO_2 nanostructures devices are defined as the ratio of the collected electrons to the incident photons. The above equation can be modified as follows

$$J_{SC}\Big/ mAcm^{-2} = \int_{\lambda_1}^{\lambda_2}\frac{P_{in\lambda}\times\lambda}{1.99\times10^{-16}}\times\frac{IPCE_{\lambda}}{100}\times\frac{1}{6.24\times10^{18}}d\lambda \qquad (5)$$

Solving above integration of both the IPCE spectra with the AM1.5 G solar photon flux yields a current density of 8.42 $mAcm^{-2}$ and 17.97 $mAcm^{-2}$ for T_{100} and T_{190} samples respectively, which is in well agreement with the measured photocurrent density from J-V curves.

Overall, the enhancement of power conversion efficiency for the 3D dendrites and 3D dendritic hollow urchin like nanostructures compared with other nanoparticulate, nanorods, nanoflowers could be attributed to the excellent surface area, effective dye loading, effective light scattering and harvesting into the 3D nanostructures.

Discussion

We have developed a novel and facile approach for exotic nanostructures of TiO_2 by simple, cost effective and surfactant free hydrothermal route for the first time using tetrabutyl titanate (TBT) precursor. The nano-morphologies were tuned from clusters of nanoparticles to 1D tetragonal nanorods pillars to 3D dendrites to 3D dendritic hollow urchin architectures by controlling preparative parameters. The deposited samples show different nanostructures containing nanorod assembly with average ~30 nm in diameter. This unique morphology has been created with an adequate combination of temperature and precursor medium. Based on these 3D dendrites and 3D dendritic hollow urchin containing bunch of aligned nanorod with 30 nm diameter show 5.32% and 7.16% conversion efficiency respectively, which is much higher than clusters of nanoparticles as well as nanorods pillars. Such type of hybrid nanostructured assembly will be also helpful for photocatalysis, lithium ion batteries, QDSSCS, hybrid polymer solar cell (HPSC), and efficient flexible dye sensitized solar cell. This approach may pave the way to synthesize better and efficient TiO_2 electrodes for respective applications at low cost.

Methods

In a typical synthesis process, 0.5 ml Titanium (IV) butoxide ($C_{16}H_{36}O_4Ti$) (Aldrich, 97%) (TBT) was dissolved in equal volume of concentrated HCl (37% Sigma Aldrich) and distilled water by magnetic stirring. The clear and transparent solution was transferred into a Teflon-lined stainless steel autoclave with a total volume of 25 mL. The fluorine doped tin oxide (FTO) coated glass substrate was then immersed into the solution parallel to the Teflon wall. The sealed autoclave was then kept in a furnace for 3 h at different temperatures. After synthesis, the autoclave was cooled to room temperature naturally. In the present investigation, the hydrothermal synthesis was conducted at various temperatures from 100°C to 190°C. The deposited samples were designated as T_{100}, T_{110}, T_{120}, T_{130}, T_{140}, T_{150}, T_{160}, T_{170}, T_{180}, and T_{190} for 100°C, 110°C, 120°C, 130°C, 140°C, 150°C, 160°C, 170°C, 180°C and 190°C respectively. The TiO_2 deposited FTO substrate was taken out, rinsed with deionized water and allowed to dry in an oven for 30 min. The fresh hydrothermal solution was prepared before each experiment. The surface morphology of the samples were recorded by a field emission scanning electron microscope (FESEM; S-4700, Hitachi). Transmission electron microscopy (TEM) micrographs, selected area electron diffraction (SAED) pattern and high-resolution transmission electron microscopy (HRTEM) images were obtained by TECNAI F20 Philips operated at 200 KV. The TEM sample was prepared by drop casting of ethanolic dispersion of TiO_2 samples onto a carbon coated Cu grid. The X-ray diffraction (XRD) measurements were carried out using a D/MAX Uitima III XRD spectrometer (Rigaku, Japan) with Cu Kα line of 1.5410 Å. The elemental information regarding the deposited TiO_2 sample was analyzed using an X-ray photoelectron spectrometer (XPS) (VG Multilab 2000-Thermo Scientific, USA, K-Alpha) with a multi-channel detector, which can endure high photonic energies from 0.1 to 3 keV.

The deposited photoelectrodes were further treated with aqueous $TiCl_4$ solution followed by annealing at 450°C. The $TiCl_4$ treated TiO_2 photoelectrodes were subsequently soaked in ethanolic 0.5 mM N719 dye (Dyesol) solution at room temperature for 24 h and then washed carefully in ethanol. A compact and sealed dye sensitized solar cell (DSSC) was fabricated using a standard two electrode configuration, comprising dye loaded Glass/FTO/TiO_2 (with an active surface area of 0.25 cm^2) as the photoanode and platinum coated FTO as the counter electrode, which is sealed with the working electrode using a thermoplastic (~1 μm). The Pt/FTO counter electrodes were prepared by commercial Pt-paste (Solaronix) using doctor blade technique. The deposited Pt/FTO substrate annealed at 450°C for 30 min in air. The iodide-based electrolyte (Dyesol) was used as the redox electrolyte and injected into the interelectrode space from the counter electrode side through a

pre-drilled hole. The cells were illuminated using a solar simulator at AM 1.5 G for 10 s, where the light intensity was adjusted with an NREL-calibrated Si solar cell with a KG-5 filter to 1 sun intensity (100 mW cm^{-2}). The incident-photon-to-current conversion efficiency (IPCE) spectra were measured as a function of wavelength from 300 nm to 1200 nm on the basis of a Spectral Products DK240 monochromator.

1. Fujishima, A. & Honda, K. Electrochemical Photolysis of Water at a Semiconductor Electrode. *Nature* **238**, 37–38 (1972).
2. Grätzel, M. Photoelectrochemical cells. *Nature* **414**, 338–344 (2001).
3. Robel, I., Kuno, M. & Kamat, P. V. Size-Dependent Electron Injection from Excited CdSe Quantum Dots into TiO_2 Nanoparticles. *J. Am. Chem. Soc.* **129**, 4136–4137 (2007).
4. Mali, S. S. *et al.* PbS quantum dot sensitized anatase TiO_2 nanocorals for quantum dot-sensitized solar cell applications. *Dalton Trans.* **41**, 6130–6136 (2012).
5. Mali, S. S. *et al.* Effective light harvesting in CdS nanoparticle-sensitized rutile TiO_2 microspheres. *Electrochim. Acta* **90**, 666–672 (2013).
6. Bai, H., Liu, Z. & Sun, D. D. A lithium-ion anode with micro-scale mixed hierarchical carbon coated single crystal TiO_2 nanorod spheres and carbon spheres. *J. Mater. Chem.* **22**, 24552–24557 (2012).
7. Liu, B. & Aydil, E. S. Growth of Oriented Single-Crystalline Rutile TiO_2 Nanorods on Transparent Conducting Substrates for Dye-Sensitized Solar Cells. *J. Am. Chem. Soc.* **131**, 3985–3990 (2009).
8. Ding, K. *et al.* Facile Synthesis of High Quality TiO_2 Nanocrystals in Ionic Liquid via a Microwave-Assisted Process. *J. Am. Chem. Soc.* **129**, 6362–6363 (2007).
9. Guo, W. *et al.* Rectangular Bunched Rutile TiO_2 Nanorod Arrays Grown on Carbon Fiber for Dye-Sensitized Solar Cells. *J. Am. Chem. Soc.* **134**, 4437–4441 (2012).
10. Liao, J.-Y., Lei, B.-X., Kuang, D.-B. & Su, C.-Y. Tri-functional hierarchical TiO_2 spheres consisting of anatase nanorods and nanoparticles for high efficiency dye-sensitized solar cells. *Energy Environ. Sci.* **4**, 4079–4085 (2011).
11. Liao, J.-Y., Lei, B.-X., Chen, H.-Y., Kuang, D.-B. & Su, C.-Y. Oriented hierarchical single crystalline anatase TiO_2 nanowire arrays on Ti-foil substrate for efficient flexible dye-sensitized solar cells. *Energy Environ. Sci.* **5**, 5750–5757 (2012).
12. Wu, W.-Q. *et al.* Hydrothermal Fabrication of Hierarchically Anatase TiO_2 Nanowire arrays on FTO Glass for Dye-sensitized Solar Cells. *Sci. Rep.* **3**, 1352–1357 (2013).
13. Lv, M. *et al.* Optimized porous rutile TiO_2 nanorod arrays for enhancing the efficiency of dye-sensitized solar cells. *Energy Environ. Sci.* **6**, 1615–1622 (2013).
14. Mali, S. S. *et al.* Hydrothermal synthesis of rutile TiO_2 nanoflowers using Brønsted Acidic Ionic Liquid [BAIL]: Synthesis, characterization and growth mechanism. *CrystEngComm* **14**, 1920–1924 (2012).
15. Mali, S. S., Betty, C. A., Bhosale, P. N. & Patil, P. S. Hydrothermal synthesis of rutile TiO_2 with hierarchical microspheres and their characterization. *CrystEngComm* **13**, 6349–6351 (2011).
16. Mali, S. S. *et al.* Efficient dye-sensitized solar cells based on hierarchical rutile TiO_2 microspheres. *CrystEngComm* **14**, 8156–8161 (2012).
17. Hosono, E., Fujihara, S., Kakiuchi, K. & Imai, H. Growth of Submicrometer-Scale Rectangular Parallelepiped Rutile TiO_2 Films in Aqueous $TiCl_3$ Solutions under Hydrothermal Conditions. *J. Am. Chem. Soc.* **126**, 7790–7791 (2004).
18. Berhe, S. A., Nag, S., Molinets, Z. & Youngblood, W. J. Influence of Seeding and Bath Conditions in Hydrothermal Growth of Very Thin (20 nm) Single-Crystalline Rutile TiO_2 Nanorod Films. *ACS Appl. Mater. Interfaces* **5**, 1181–1185 (2013).
19. Cheng, H. M., Ma, J. M., Zhao, Z. G. & Qi, L. M. Hydrothermal Preparation of Uniform Nanosize Rutile and Anatase Particles. *Chem. Mater.* **7**, 663–671 (1995).
20. Kumar, A., Madaria, A. R. & Zhou, C. W. Growth of Aligned Single-Crystalline Rutile TiO_2 Nanowires on Arbitrary Substrates and Their Application in Dye-Sensitized Solar Cells. *J. Phys. Chem. C* **114**, 7787–7792 (2010).
21. Mali, S. S. *et al.* Single-step synthesis of 3D nanostructured TiO_2 as a scattering layer for vertically aligned 1D nanorod photoanodes and their dye-sensitized solar cell properties. *CrystEngComm* **15**, 5660–5667 (2013).
22. Yu, J. G., Fan, J. J. & Lv, K. L. Anatase TiO_2 nanosheets with exposed (001) facets: improved photoelectric conversion efficiency in dye-sensitized solar cells. *Nanoscale* **2**, 2144–2149 (2010).
23. Wu, X., Chen, Z., Lu, G. Q. & Wang, L. Solar cells: nanosized anatase TiO_2 single crystals with tunable exposed (001) facets for enhanced energy conversion efficiency of dye-Sensitized Solar Cells. *Adv. Funct. Mater.* **21**, 4166–4166 (2011).
24. Jung, M. H., Chu, M. J. & Kang, M. G. TiO_2 nanotube fabrication with highly exposed (001) facets for enhanced conversion efficiency of solar cells. *Chem. Commun.* **48**, 5016–5018 (2012).
25. Sun, Z. *et al.* Rational Design of 3D Dendritic TiO_2 Nanostructures with Favorable Architectures. *J. Am. Chem. Soc.* **133**, 19314–19317 (2011).
26. Sun, Z. *et al.* Continually adjustable oriented 1D TiO_2 nanostructure arrays with controlled growth of morphology and their application in dye-sensitized solar cells. *CrystEngComm* **14**, 5472–5478 (2012).
27. Sun, Z., Kim, J. H., Zhao, Y., Attard, D. & Dou, S. X. Morphology-controllable 1D–3D nanostructured TiO_2 bilayer photoanodes for dye-sensitized solar cells. *Chem. Comm.* **49**, 966–968 (2013).
28. Dennler, G., Scharber, M. C. & Brabec, C. J. Polymer-Fullerene Bulk-Heterojunction Solar Cells. *Adv. Mater.* **21**, 1323–1338 (2009).

Acknowledgments

This work was supported by Basic Science Research Program through the National Research Foundation of Korea (NRF) funded by the Ministry of Education (NRF-2009-0094055).

Author contributions

S.S.M. & C.K.H. contributed to the conception and design of the experiments, analysis of the data and writing the paper. S.S.M. carried out all experiments and wrote the paper. S.S.M., H.J.K. and C. S. S. performed J-V, IPCE measurement, calculations and analyzed data. P.S.P. and J.H.K. participated in the scientific discussion and valuable suggestions during the course of this manuscript. All authors discussed the results and reviewed the manuscript.

Additional information

Supplementary information accompanies this paper at http://www.nature.com/scientificreports

Competing financial interests: The authors declare no competing financial interests.

How to cite this article: Mali, S.S. *et al.* Surfactant free most probable TiO_2 nanostructures via hydrothermal and its dye sensitized solar cell properties. *Sci. Rep.* **3**, 3004; DOI:10.1038/srep03004 (2013).